ChemPubSoc Europe

DOI: 10.1002/celc.201800639

CHEMELECTROCHEM Articles

Sn_4P_3/SbSn Nanocomposites for Anode Application in Sodium-Ion Batteries

Danni Lan[a] and Quan Li*[a]

A facile one-pot solvothermal method has been developed to synthesize Sn_4P_3/SbSn nanocomposites with a side-by-side configuration in individual nanoparticles. We show that introducing SbSn to Sn_4P_3 in such a configuration can improve the cyclic stability of the phase-pure Sn_4P_3 electrode without sacrificing its practical capacity, although the theoretical capacity of SbSn is lower than that of Sn_4P_3. The nanocomposite anode delivers a highest capacity of 614.7 mA h g^{-1} at a current density of 100 mA g^{-1} and shows superior capacity retention to the phase pure Sn_4P_3, SbSn, or physical mixture of Sn_4P_3&SbSn based anodes after long cycles. The intact interface between the Sn_4P_3 and SbSn in the nanocomposite and their synergetic effect play important roles in enhancing the electrochemical performance of the composite electrode.

1. Introduction

Tin phosphide (Sn_4P_3) is a promising anode in sodium ion batteries (SIBs), due to its high theoretical capacity of 1131 mA h g^{-1} and reasonably low redox potential (~0.3–0.6 V vs. Na/Na^+), as well as the low cost of both Sn and P.[1–12] However, phase pure Sn_4P_3 suffers from poor cyclic stability, as commonly ascribed to a number of factors, including the volume expansion induced electrode pulverization and large stress that limits the Na dynamics, and the chemical instability in the electrode (e.g., solid electrolyte interphase (SEI), sodiated phases of Na–P, and tin segregation during charging/discharging).[13–16]

Introducing an appropriate second phase to form composite with Sn_4P_3 would be an effective approach to improve the electrochemical performance of the electrode, if it can help to buffer the volume expansion and at the same time stabilize various species in the electrode. Carbon materials are the most commonly employed ones for such a purpose. A best performance of Sn_4P_3/C composite electrode has been demonstrated in Sn_4P_3-P@Graphene nanocomposite (30 wt.% graphene) with a stable capacity of ~840 mA h g^{-1} (calculated based on mass of Sn and P, excl. graphene) at 0.2 A g^{-1} over 200 cycles.[17] The major problems associated with the carbon based composite system are the low capacity of the carbon materials (< 300 mA h g^{-1}) and its low density (e.g., graphite < 1 g cm^{-3})[18], resulting in low volumetric capacity of the composite electrodes.[19] Alternatively, composting Sn_4P_3 with other active material of high capacity is a feasible method, so that the cycle stability of the electrode can be improved without much sacrificing the capacity. Such material candidates are desired to have high theoretical capacity, density, stability and reasonable redox potential. In this regard, metallic alloy SbSn serves as a promising choice, due to its high density (13.827 g cm^{-3} for SbSn alloy[20] vs. 5.870 g cm^{-3} for Sn_4P_3[21]), relatively high capacity (theoretical capacity of 754 mA h g^{-1}), reasonable redox potential (< 1 V) and reasonable stability (being better than individual Sb, Sn anodes).[22,23]

In the present work, we have synthesized the Sn_4P_3/SbSn nanocomposites by a facile one-pot solvothermal method. Sn_4P_3 and SbSn form a side-by-side structure in individual nanocomposite particles. When used as anode material for SIBs, they show enhanced performance compared to the phase pure Sn_4P_3, SbSn and physical mixture of Sn_4P_3&SbSn anodes. It can deliver a highest capacity of 614.7 mA h g^{-1} and maintains a capacity retention of 74% after 100 cycles at a current density of 100 mA g^{-1}. Contributing factors to the superior electrochemical performance of the Sn_4P_3/SbSn nanocomposites are discussed, and we show that the overall performance benefits from not only the intact interface between the Sn_4P_3 and SbSn, but also the synergetic effect of the Sn_4P_3 and SbSn phases in the nanocomposite during sodiation/desodiation.

2. Results and Discussion

Figure 1a shows the X-ray diffraction (XRD) patterns of the as-prepared Sn_4P_3/SbSn nanocomposites. Two sets of peaks are identified and they can be respectively indexed to rhombohedral Sn_4P_3 (JCPDS # 73-1820) and SbSn (JCPDS # 33-118). No other peak is found. The XRD result suggests the coexistence of phase pure Sn_4P_3 and SbSn without other crystalline impurity phases. Figure 1b shows a scanning electron microscopy (SEM) image of the Sn_4P_3/SbSn composite nanoparticles. They have spherical-like morphology with faceted surfaces. Their sizes are in the range of several tens to hundreds of nanometers. The Sn/P/Sb ratio of these composite nanoparticles is estimated to be 54:34:12, based on the energy-dispersive X-ray spectroscopy (EDS) results taken from nanoparticle ensembles (Figure 1c). Transmission electron microscopy (TEM) based techniques are employed to investigate the detailed microstructure of

[a] Dr. D. Lan, Prof. Q. Li
Department of Physics
The Chinese University of Hong Kong
Shatin, New Territory, Hong Kong, China
E-mail: liquan@phy.cuhk.edu.hk

Supporting information for this article is available on the WWW under https://doi.org/10.1002/celc.201800639

© 2018 Wiley-VCH Verlag GmbH & Co. KGaA, Weinheim

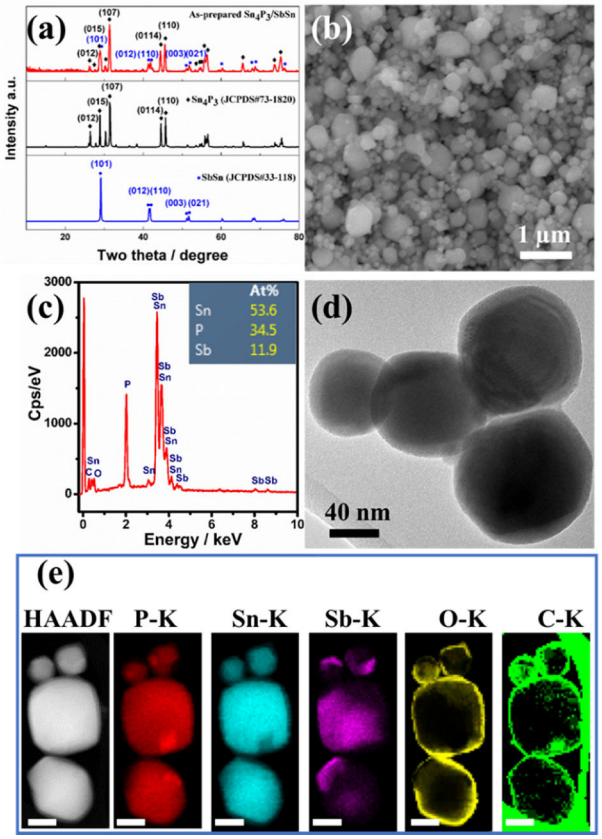

Figure 1. a) XRD; b) SEM; c) EDS; d) low-magnification TEM image; e) STEM-EDS/EELS maps of the Sn_4P_3/SbSn nanocomposites, scale bar is 100 nm.

the Sn_4P_3/SbSn nanocomposites. Figure 1d first shows a low magnification TEM image, in which a thin surface layer (of ~5 nm) can be observed in each of the nanoparticles. Element mapping taken in the STEM model further reveals the spatial distribution of the compositional elements in the as-prepared samples. One can tell that enrichment of Sn–P and Sn–Sb occurs in different part of the nanoparticles, while O, C and some P are confined in the surface region of the same nanoparticle (Figure 1e). The surface C–O/P–C materials come from the organic solvent capping as well as adsorption of the organic by-product during synthesis.[8]

There are several critical stages in the Sn_4P_3/SbSn nanocomposite formation. A schematic is shown in Figure 2 to illustrate the growth mechanism of the Sn_4P_3/SbSn nanocomposites. Both Sb^{3+} and Sn^{2+} can be reduced by TOP (trioctylphosphine), but the Sb particles are the first to appear due to the higher redox potential of the Sb^{3+} than that of the Sn^{2+} ions (E^{Θ} (Sb^{3+}/Sb = 0.241 V vs. standard hydrogen electrode (SHE)) and E^{Θ} (Sn^{2+}/Sn = −0.138 V vs. SHE))[24] (Figure S1, green line in the XRD pattern). With temperature increasing, reduction of the Sn^{2+} becomes more complete. After that, alloying of the Sb and Sn takes place and complete consumption of the Sb to form SbSn leads to formation of Sn/SbSn composites (Figure S1, red XRD pattern and Figure S2, STEM mapping). The concentration of the Sn sources is five times than the Sb sources (as shown above in Figure 1c), apart from those alloyed with the Sb, there remains a large amount of Sn. The unreacted Sn serve as catalyst to facilitate the cleavage of the P–C bond of the TOP, and the decomposed P sources then diffuse into Sn to form a stable Sn_4P_3 phase upon supersaturation. Continuous growth of Sn_4P_3 exhausts the rest of Sn in Sn/SbSn nanoparticles, resulting in Sn_4P_3/SbSn nanocomposites with side by side structure (Figure S1, blue XRD pattern).

The as prepared Sn_4P_3/SbSn nanocomposites are used as anodes for sodium ion half cells. Figure 3a shows the cyclic voltammograms (CV) of the Sn_4P_3/SbSn nanocomposites. Three peaks at ~1, ~0.38, ~0.05 V are obtained in the initial cathodic

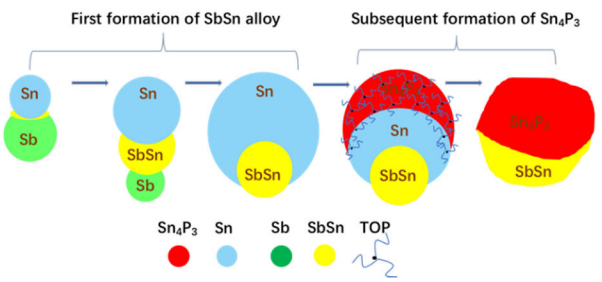

Figure 2. Schematic illustration of the growth process of the Sn_4P_3/SbSn nanocomposites.

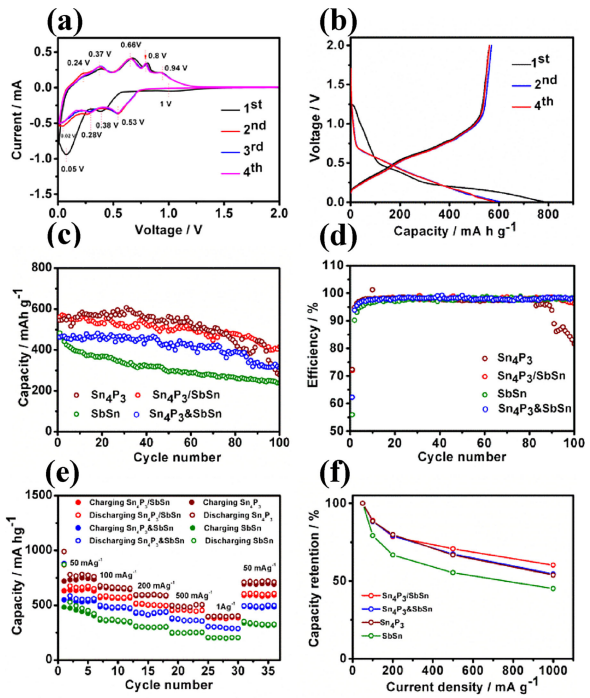

Figure 3. a) CV plots of the Sn_4P_3/SbSn nanocomposites anodes scanned at a rate of 0.05 mV s^{-1} in the voltage range of 0.01–2 V; b) charge/discharge curves of the Sn_4P_3/SbSn nanocomposites anodes at a constant current density of 100 mA g^{-1}; c) comparison of the reversible capacities of the phase pure Sn_4P_3, phase pure SbSn, Sn_4P_3&SbSn physical mixture and Sn_4P_3/SbSn nanocomposites electrodes at a current rate of 100 mA g^{-1}; d) their corresponding columbic efficiency; e) charge/discharge capacities of those electrodes measured at current densities of 50, 100, 200, 500 and 1000 mA g^{-1}; f) their corresponding capacity retentions.

© 2018 Wiley-VCH Verlag GmbH & Co. KGaA, Weinheim

scan, being ascribed to the formation of SEI (~1 V), the initial sodiation of Sb, P to Na_3Sb, Na_3P (~0.38 V), and the formation of Sn–Na alloy (~0.05 V). During the anodic scans, reproducible peaks at ~0.24, ~0.37, ~0.66, ~0.8. ~0.94 V are observed. According to the literature,[10,25–28] peaks at ~0.24, ~0.37 V mainly come from desodiation of Na–Sn alloy while the rest originate from the desodiation of Na_3P and Na_3Sb. In the second and later cathodic cycles, three stable peaks at ~0.53, ~0.28, ~0.02 V can be found, which are assigned to the stepwise sodiation of Sb, P and Sn. The initial cathodic scan/sodiation process contains not only the reduction of the SbSn and Sn_4P_3, but also the formation of the SEI film from the electrolyte decomposition. The initial sodiation could be considered as a pre-reaction that the initial cathodic peaks are different from that in the later cycles.[29] Figure 3b plots the capacity-voltage profiles of the Sn_4P_3/SbSn nanocomposites, which deliver a discharging capacity of 779.2 mA h g^{-1} and a reversible charging capacity of 560.9 mA h g^{-1} with an initial columbic efficiency of 72% at a current density of 100 mA g^{-1}. The irreversible capacity is ascribed to the formation of the SEI.

The cycle performance of the as-prepared Sn_4P_3/SbSn nanocomposites is compared to those of the electrodes made of phase pure Sn_4P_3 nanotops, or SbSn nanoparticles obtained by dissolving the Sn_4P_3 in the Sn_4P_3/SbSn nanocomposites (Figure S3), or a physical mixture of Sn_4P_3 nanotops and SbSn nanoparticles. Figure 3c and 3d plot the cycle performance, and their corresponding columbic efficiency, respectively. Sn_4P_3/SbSn nanocomposites and phase pure Sn_4P_3 nanotops show similar initial capacity of 561 and 545 mA h g^{-1}, respectively, but a longer cycle stability is obtained in the Sn_4P_3/SbSn nanocomposites than Sn_4P_3 nanotops (capacity retention of 74% vs. 51% after 100 cycles). As a comparison, both SbSn and mixed Sn_4P_3&SbSn samples have rather low initial capacities (482.6 and 463 mA h g^{-1}, respectively,). They respectively deliver capacity retentions of 49% and 67.5% at the end of 100 cycles. Figure 3e and 3f further compare the rate performance of those four electrodes at current densities of 50, 100, 200, 500 and 1000 mA g^{-1}. The overall rate performance of the Sn_4P_3/SbSn nanocomposites is the best among all samples, although its improvement from Sn_4P_3 sample is not significant.

The above experimental results suggest that formation of Sn_4P_3/SbSn nanocomposites leads to improved rate performance and cycle stability of the electrode without sacrificing the capacity (as compared to those of phase pure Sn_4P_3 electrode). Two factors mainly contribute to the superior electrochemical properties of the Sn_4P_3/SbSn nanocomposite. Firstly, for the cycle stability, the presence of two phases (Sn_4P_3 and SbSn) leads to synergetic effect during sodiation/desodiation of the nanocomposite. The experimental results shown that Sn_4P_3 suffers from inferior cycle stability (low capacity retention after long cycles, Figure 3c). By combining Sn_4P_3 and SbSn together, the stability of the ternary electrode can be enhanced. Comparing to a single binary compound (Sn_4P_3), sodiation of the ternary electrodes involves redox reactions occurring in a range of voltages. When one of the reactions takes place, other phases serve as more effective buffer matrix to disperse the reacting phase and release stress generated from the associated volume expansion, leading to enhanced stability upon cycling. Secondly, intact interface between Sn_4P_3 and SbSn is important to facilitate sodiation kinetic during cycling. It has been reported that atomic diffusion within the Na–Sn–Sb phase during SbSn sodiation is insufficient to achieve long-range crystallization of Na_3Sb at room temperature.[28] Indeed, the crystalline phase of Na_3Sb has been observed in neither SbSn nor Sn_4P_3&SbSn physical mixture samples (Figure S4). Nevertheless, apparent Na_3Sb crystalline peaks are observed in the Sn_4P_3/SbSn nanocomposites, suggesting an improved kinetic in such a sample. Consistent observation has also been made in the corresponding CV profiles (Figure S5), i.e., sodiation peak features are more profound in the Sn_4P_3/SbSn nanocomposite than in the Sn_4P_3&SbSn mixture, especially for the peak at ~0.8 V (mainly due to the reaction between the Na and Sb). From the electrochemical impedance spectroscopy (EIS) results, the low surface/charge transfer resistance and fast intra-solid diffusivity further confirm the fast kinetic of the Sn_4P_3/SbSn nanocomposite (Figure S6). The improved sodiation kinetic results in a better rate performance of the nanocomposite electrode.

3. Conclusions

In conclusion, we have synthesized the Sn_4P_3/SbSn nanocomposite by a one-pot solvothermal method. During the reaction, Sb is first reduced and then alloys with the later formed Sn to form Sn/SbSn heterostructure. The elemental Sn sources in the Sn/SbSn heterostructure then serve as catalyst to guide the growth of the Sn_4P_3, resulting in Sn_4P_3/SbSn nanocomposites with side by side structure. When used as anodes for sodium ion batteries, these composites show superior electrochemical performance to those of phase pure Sn_4P_3, SbSn and physically mixed Sn_4P_3&SbSn anodes. It can deliver a stable reversible capacity of 415 mA h g^{-1} after 100 cycles with high rate performance (a capacity of 388 mA h g^{-1} at 1 A g^{-1}). The high electrochemical performance would come from the intact interface between the Sn_4P_3 and SbSn, which facilitates the reaction kinetic during sodiation/desodiation. The synergetic effect of Sn_4P_3 and SbSn, which ensures a mutual buffering effect during electrochemical reaction, also contribute to the enhanced stability of the Sn_4P_3/SbSn nanocomposites.

Experimental Section

Materials Preparation and Characterization

Synthesis of the Sn_4P_3/SbSn Nanocomposites, SbSn Samples, Sn_4P_3 Nanotops and Sn_4P_3&SbSn Mixture

The as-prepared Sn_4P_3/SbSn nanocomposites were obtained under one pot reaction in an atmosphere of high purity of nitrogen. In details, 5 mmol tin(II) acetylacetonate, 20 mL trioctylphosphine (TOP), and 1 mmol antimony (III) acetate were mixed and degassed at 120 °C for 0.5 h by heating mantle in a flask under stirring with a reflux condenser and then rising the temperature to 350 °C and

© 2018 Wiley-VCH Verlag GmbH & Co. KGaA, Weinheim

aged for 3 h. After cooling down to room temperature, samples were washed and centrifuged with hexane for four times. The final powers were obtained by vacuum-drying.

SbSn samples were obtained by removing the Sn_4P_3 part in the Sn_4P_3/SbSn nanocomposites with 6 mol/L HCl solution and then washed and centrifuged with DI-water and ethanol for four times. The final powers were obtained by vacuum-drying.

Sn_4P_3 nanotops were synthesized according to the approach in our previous work published elsewhere.[8]

Sn_4P_3&SbSn mixture were made by hand grinding the Sn_4P_3 nanotops and SbSn samples together.

Characterization

X-ray diffraction (XRD, SmartLab, Rigaku) with a Cu–Kα radiation source ($\lambda = 0.1541$ nm) was used to characterize the crystallinity and phases of the samples. A scanning electron microscope (SEM, JSM-7800F, JEOL) was performed to reveal the morphological and compositional analyses. Transmission electron microscopy (TEM) based techniques were carried out using a Tecnai F20 ST (FEI) microscope operating at 200 kV. Element mapping taken in STEM model was performed by using energy-dispersive X-ray spectroscopy (EDS) and electron energy loss spectroscopy (EELS) simultaneously. Sb, Sn, P maps were obtained by EDS while C and O maps were taken at the C and O K edge by EELS.

Assembly of a 2032 Coin-Type Half-Cell with Na as the Anode

Active materials (the Sn_4P_3/SbSn nanocomposites, phase pure Sn_4P_3, SbSn or Sn_4P_3&SbSn mixture) were mixed with multi-walled carbon nanotubes (MWCNTs) and sodium carboxymethyl cellulose (CMC) at the weight ratio of 70:20:10 in distilled water to form a slurry and then coating the slurry on copper foil to a thin film. After vacuum drying at 60 °C overnight, the film was cut for electrode assembling. The mass loading of Sn_4P_3/SbSn nanocomposites was ~1 mg cm^{-2}. The electrolyte consisted of 1 M $NaClO_4$ in propylene carbonate (PC)/fuoroethylene carbonate (FEC) (95:5, by vol.). Galvanostatic charge–discharge cycling tests were performed with a Land CT2001A battery testing system (Land, P. R. China) at room temperature. Cyclic voltammetry (CV) scanned at a sweep rate of 0.05 mV/s and electrochemical impedance spectroscopy (EIS) were performed on a CHI660c electrochemical workstation (ChenHua instrument Co., China).

Acknowledgements

This work is supported by the RGC/GRF under project No. 14316716.

Conflict of Interest

The authors declare no conflict of interest.

Keywords: tin phosphide · antimony tin alloy · nanocomposites · sodium-ion batteries

[1] Y. Kim, Y. Kim, A. Choi, S. Woo, D. Mok, N. S. Choi, Y. S. Jung, J. H. Ryu, S. M. Oh, K. T. Lee, *Adv. Mater.* **2014**, *26*, 4139–4144.
[2] J. Qian, Y. Xiong, Y. Cao, X. Ai, H. Yang, *Nano Lett.* **2014**, *14*, 1865–1869.
[3] J. Liu, P. Kopold, C. Wu, P. A. van Aken, J. Maier, Y. Yu, *Energy Environ. Sci.* **2015**, *8*, 3531–3538.
[4] H. Usui, T. Sakata, M. Shimizu, H. Sakaguchi, *Electrochemistry* **2015**, *83*, 810–812.
[5] Q. Li, Z. Li, Z. Zhang, C. Li, J. Ma, C. Wang, X. Ge, S. Dong, L. Yin, *Adv. Energy Mater.* **2016**, *6*, 1600376.
[6] L. Zheng, R. A. Dunlap, M. N. Obrovac, *J. Electrochem. Soc.* **2016**, *163*, A1188–A1191.
[7] X. Fan, T. Gao, C. Luo, F. Wang, J. Hu, C. Wang, *Nano Energy* **2017**, *38*, 350–357.
[8] D. Lan, W. Wang, L. Shi, Y. Huang, L. Hu, Q. Li, *J. Mater. Chem. A* **2017**, *5*, 5791–5796.
[9] L. Ma, P. Yan, G. Zhu, Y. Shen, *J. Mater. Chem. A* **2017**, *5*, 16994–17000.
[10] H. Usui, Y. Domi, K. Fujiwara, M. Shimizu, T. Yamamoto, T. Nohira, R. Hagiwara, H. Sakaguchi, *ACS Energy Lett.* **2017**, *2*, 1139–1143.
[11] J. M. Wenchao Zhang, W. Kong Pang, Z. Guo, Z. Chena, *Electrochim. Acta*, **2017**, *235*, 107–113.
[12] S. C. Jung, J.-H. Choi, Y.-K. Han, *J. Mater. Chem. A* **2018**, *6*, 1772–1779.
[13] J. Y. Jang, Y. Lee, Y. Kim, J. Lee, S.-M. Lee, K. T. Lee, N.-S. Choi, *J. Mater. Chem. A* **2015**, *3*, 8332–8338.
[14] S. Liu, H. Zhang, L. Xu, L. Ma, X. Chen, *J. Power Sources* **2016**, *304*, 346–353.
[15] J. Mao, X. Fan, C. Luo, C. Wang, *ACS Appl. Mater. Interfaces* **2016**, *8*, 7147–7155.
[16] H. S. Shin, K. N. Jung, Y. N. Jo, M. S. Park, H. Kim, J. W. Lee, *Sci. Rep.* **2016**, *6*, 26195.
[17] Y. Xu, B. Peng, F. M. Mulder, *Adv. Energy Mater.* **2017**, *8*, 1701847.
[18] I. T. Kim, E. Allcorn, A. Manthiram, *J. Power Sources* **2015**, *281*, 11–17.
[19] S. Liu, J. Feng, X. Bian, J. Liu, H. Xu, Y. An, *Energy Environ. Sci.* **2017**, *10*, 1222–1233.
[20] G. Hägg, A. G. Hybinette, *The London, Edinburgh, and Dublin Philosophical Magazine and Journal of Science* **1935**, *20*, 913–929.
[21] O. Olofsson, *Acta Chem. Scand.* **1970**, *24*, 1153–1162.
[22] L. Xiao, Y. Cao, J. Xiao, W. Wang, L. Kovarik, Z. Nie, J. Liu, *Chem. Commun.* **2012**, *48*, 3321–3323.
[23] M. Walter, S. Doswald, M. V. Kovalenko, *J. Mater. Chem. A* **2016**, *4*, 7053–7059.
[24] Z. Yi, Q. Han, D. Geng, Y. Wu, Y. Cheng, L. Wang, *J. Power Sources* **2017**, *342*, 861–871.
[25] H. Usui, Y. Domi, S. Ohshima, H. Sakaguchi, *Electrochim. Acta* **2017**, *246*, 280–284.
[26] H. Usui, Y. Domi, R. Yamagami, K. Fujiwara, H. Nishida, H. Sakaguchi, *ACS Appl. Energy Mater.* **2018**, *1*, 306–311.
[27] L. D. Ellis, T. D. Hatchard, M. N. Obrovac, *J. Electrochem. Soc.* **2012**, *159*, A1801-A1805.
[28] L. Baggetto, H.-Y. Hah, J.-C. Jumas, C. E. Johnson, J. A. Johnson, J. K. Keum, C. A. Bridges, G. M. Veith, *J. Power Sources* **2014**, *267*, 329–336.
[29] S. Huang, C. Meng, M. Xiao, S. Ren, S. Wang, D. Han, Y. Li, Y. Meng, *Sustainable Energy Fuels* **2017**, *1*, 1944–1949.

Manuscript received: May 14, 2018
Accepted Article published: June 11, 2018
Version of record online: ■■, ■■■

© 2018 Wiley-VCH Verlag GmbH & Co. KGaA, Weinheim

ARTICLES

Better together: Sn_4P_3/SbSn nanocomposites are synthesized, which exhibit a superior electrochemical performance to binary Sn_4P_3-based anodes when used for sodium ion batteries.

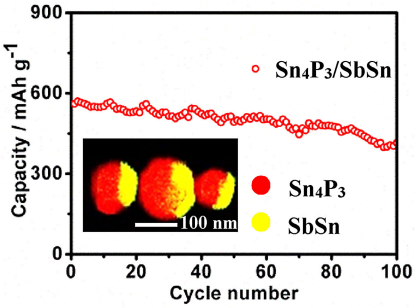

*Dr. D. Lan, Prof. Q. Li**